

Zonal Flows and Electromagnetic Drift Wave Turbulence

Bruce D. Scott

Max-Planck-IPP, EURATOM Association, 85748 Garching, Germany

Jul 2002

Detailed computations of tokamak edge turbulence in three dimensional, globally consistent flux tube geometry show an inhibition of the standard scenario in which zonal ExB flows generated by the turbulence should lead to transport barrier formation. It is found by comparison to slab geometry and by analysis of the energetics that the zonal flow energy is depleted by toroidal coupling to the pressure through the geodesic curvature. Edge transport barriers would then depend on the physics of the neoclassical equilibrium.

PACS numbers: 52.25.Fi 91.25.Cw 52.30.-q 52.40.Nk

Drift Wave Turbulence and Zonal Flows. Drift wave turbulence is nonlinear, nonperiodic motion involving disturbances on a background thermal gradient of a magnetised plasma and eddies of fluid like motion in which the advecting velocity of all charged species is the ExB velocity [1,2]. The disturbances in the electric field implied by the presence of these eddies are caused by the tendency of the electron dynamics to establish a force balance along the magnetic field. Pressure disturbances have their parallel gradients balanced by a parallel electric field, whose static part is given by the parallel gradient of the electrostatic potential. This potential in turn is the stream function for the ExB velocity in drift planes, which are locally perpendicular to the magnetic field. The turbulence is driven by the background gradient, and the electron pressure and electrostatic potential are coupled together through parallel currents. Departures from the static force balance are mediated primarily through electromagnetic induction and resistive friction, but also the electron inertia, which is not negligible [3]. Further details are provided by the temperatures, whose dynamics is very robust due to nonlinear, time dependent Landau damping. In a three dimensional, toroidal flux surface geometry, the turbulence is characterised by a nonlinear instability whose inherent vorticity is strong enough to “supersede” linear interchange instabilities, giving tokamak edge turbulence a drift wave basic character [4].

Although this turbulence effects an unsteady transport through nonlinear advection of the thermodynamic state variables, actual modification of the profiles proceeds on the much slower transport time scale, typically at least three orders of magnitude slower than the turbulence even in steep gradient regions. Such quasilinear modification of the background (a three wave interaction involving a wave and its complex conjugate driving changes in the background) also occurs in the other variables, specifically the ExB vorticity, for which the time scale is short enough for a self-consistent interaction with the turbulence to affect the dynamics of the turbulence itself. These are the “zonal flows” [5], which are simply the ExB flows resulting from disturbances in the electrostatic potential which are constant on a given magnetic flux surface. One can think of a zonal flow as a rigid poloidal rotation of the entire flux surface. These flows are important because when and where they are sheared they can cause a local suppression of the turbulence. Suppression of turbulence by sheared flows began by considering an imposed flow which is part of the background [6]. It was then pointed out that the process by which this suppression occurs conserves energy, mainly involving a transfer of energy in three wave interactions from smaller scale eddies and the larger scale background [7], a variant of the more general inverse energy cascade from smaller to larger scales in two dimensional, incompressible turbulence [8]. Suppression by imposed ExB shear was then shown in computations to proceed energetically [9]. Self consistent interactions concern time dependent zonal flows which have time and space

scales comparable to or only somewhat larger than those of the turbulence. Their study as such [10], followed global scale computational studies showing them to be very important in limiting the radial scale of the turbulence and consequently the resulting transport [11]. Their importance in fusion research lies in the fact that zonal ExB flow (electric field) shear is thought to underly the transition and maintenance of the H-mode operation of tokamak confinement [12].

We here examine the physics of the zonal flow/turbulence interaction in a model of the turbulence which includes two important generalisations: departures from the “adiabatic” state of perfect electron force balance, and an electromagnetic character in that response, which allows significant delays in the adiabatic response at larger perpendicular scales, since the collisional response is through the parallel current, while the inductive response is through the time dependence of the parallel magnetic potential (by Ampere’s law, the current is given by the perpendicular Laplacian of that potential). We will find that in toroidal geometry, although the drive of the zonal flows via Reynolds stress remains, the geodesic curvature of the magnetic field lines couples the zonal flows to pressure sidebands with finite parallel gradient. These sidebands serve as a localised part of the general source for the turbulence, as the free energy transfer in the pressure disturbances is preferentially towards smaller scales. The build up of strong, long lived ExB “mean flow” shear layers is thereby inhibited, preventing the turbulence from self consistently generating enough ExB shear to strongly reduce its own amplitude. This prevents the scenario in which the zonal flow drive process should lead to transport barrier formation. In slab geometry, the geodesic curvature effect is absent and mean flows do develop, but we find by inserting specifically this geodesic curvature effect that the toroidal result is recovered (incidentally demonstrating the weakness of the ballooning/interchange effect in the turbulence). It is important to note in this context that models of transport barrier formation by Reynolds stress-induced self-generated flows rely on two-dimensional slab geometry [13], and they work well in such computations [14], but the three-dimensional toroidal result is rather different as documented herein.

The DALF3 Model. The simplest three dimensional model of drift wave dynamics which takes the self consistent adiabatic response into account and allows it an electromagnetic character is a four field model in toroidal flux tube geometry called DALF3 (the drift Alfvén model [3] but omitting the temperature dynamics). The state variables are the electrostatic potential $\tilde{\phi}$ and the electron pressure \tilde{p}_e , and the flux variables are the parallel current \tilde{J}_{\parallel} and the parallel ion velocity \tilde{u}_{\parallel} , all expressed as disturbances on the equilibrium which is a set of constant parameters except where the ExB and magnetic nonlinearities operate on the background gradients. In the Ohm’s law, electromagnetic induction, electron inertia,

and resistive friction are all retained. The adiabatic response is the reaction of the parallel current, controlled by those three effects, to the pressure/potential static force imbalance, acting to couple \tilde{p}_e and $\tilde{\phi}$ through the shear Alfvén dynamics. The model equations in simplified sheared flux tube geometry are

$$\frac{n_e M_i c^2}{B^2} \frac{d}{dt} \nabla_{\perp}^2 \tilde{\phi} = B \nabla_{\parallel} \frac{\tilde{J}_{\parallel}}{B} + \nabla \cdot \frac{c}{B^2} \mathbf{B} \times \nabla \tilde{p}_e \quad (1)$$

$$\frac{1}{c} \frac{\partial \tilde{A}_{\parallel}}{\partial t} + \frac{m_e}{n_e e^2} \frac{d \tilde{J}_{\parallel}}{dt} + \eta_{\parallel} \tilde{J}_{\parallel} = \frac{1}{n_e e} \nabla_{\parallel} (p_e + \tilde{p}_e) - \nabla_{\parallel} \tilde{\phi} \quad (2)$$

$$\frac{d}{dt} (\tilde{p}_e + p_e) = \frac{T_e}{e} B \nabla_{\parallel} \frac{\tilde{J}_{\parallel}}{B} - p_e B \nabla_{\parallel} \frac{\tilde{u}_{\parallel}}{B} - \frac{1}{e} \nabla \cdot \frac{c}{B^2} \mathbf{B} \times \nabla \tilde{p}_e + p_e \nabla \cdot \frac{c}{B^2} \mathbf{B} \times \nabla \tilde{\phi} \quad (3)$$

$$n_e M_i \frac{d \tilde{u}_{\parallel}}{dt} = -\nabla_{\parallel} (p_e + \tilde{p}_e) \quad (4)$$

with Ampere's law $\tilde{J}_{\parallel} = -(c/4\pi) \nabla_{\perp}^2 \tilde{A}_{\parallel}$. The ExB advective and parallel derivatives are given by

$$\frac{d}{dt} = \frac{\partial}{\partial t} + \frac{c}{B^2} \mathbf{B} \times \nabla \phi \cdot \nabla \quad \nabla_{\parallel} = \frac{1}{B} \mathbf{B} \cdot \nabla - \frac{c}{B^2} \mathbf{B} \times \nabla \frac{1}{c} \tilde{A}_{\parallel} \cdot \nabla \quad (5)$$

where \mathbf{B} and B are the equilibrium magnetic field and its magnitude, and the combinations involving $\tilde{\phi}$ and \tilde{A}_{\parallel} give the ExB and disturbed parallel derivatives, respectively, i.e., the nonlinearities. The flux tube geometry used is detailed elsewhere [15], as is the importance of global consistency which controls field line connection [16]. The standard normalisation is in terms of the drift scale $\rho_s = c_s/\Omega_i$ and frequency c_s/L_{\perp} , where $c_s^2 = T_e/M_i$ and $\Omega_i = eB/M_i c$, and L_{\perp} is the background scale length for p_e . The parameters controlling the adiabatic response are $\hat{\beta} = (c_s/L_{\perp})^2 (qR/v_A)^2$, and $\hat{\mu} = (c_s/L_{\perp})^2 (qR/V_e)^2$, and $C = 0.51(\nu_e L_{\perp}/c_s) \hat{\mu}$, reflecting the competition between perpendicular ExB turbulence and the parallel dynamics, where the field line connection length is $2\pi qR$, V_e is the electron thermal velocity ($V_e^2 = T_e/m_e$) and the 0.51 comes from the parallel resistivity, $\eta_{\parallel} = 0.51 m_e \nu_e / n_e e^2$ [17]. The sound waves are controlled by $\hat{\epsilon} = (c_s/L_{\perp})^2 (qR/c_s)^2$, just the parallel/perp scale ratio. The effects of magnetic curvature (the radius of curvature is R , the toroidal major radius), entering through $\mathcal{K} \equiv \nabla \cdot (c/B^2) \mathbf{B} \times \nabla$ are controlled by $\omega_B = 2L_{\perp}/R$, which can be set independently — slab geometry is $\omega_B = 0$. The coordinates are $\{x, y, s\}$, representing the down-gradient, electron drift, and parallel directions, respectively. The computations are set up exactly as detailed in [15], with a grid of $64 \times 256 \times 16$ nodes in $\{x, y, s\}$, and with node spacings $h_x = h_y = 20\pi \rho_s/64$ and $h_s = 2\pi qR/16$. Nominal

parameters corresponding to a typical plasma edge in the L-mode of tokamak operation are

$$\hat{\beta} = 2 \quad \hat{\mu} = 5 \quad C = 7.65 \quad \omega_B = 0.05 \quad \hat{\epsilon} = 18350 \quad \hat{s} = 1 \quad (6)$$

roughly reflecting physical parameters:

$$n_e = 4.5 \times 10^{13} \text{ cm}^{-3} \quad T_e = 80 \text{ eV} \quad B = 2.5 \text{ T} \quad (7)$$

$$R = 165 \text{ cm} \quad L_{\perp} = 3.65 \text{ cm} \quad q = 3 \quad (8)$$

This is rather strongly collisional (standard parameter $\nu_* = 40$), but because $C\omega_B < 1$ it is still well within the drift wave regime [18].

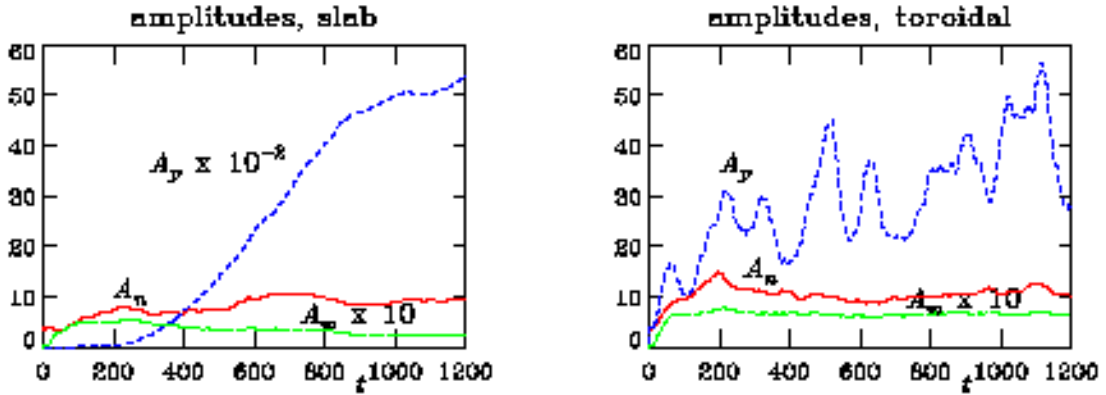


Figure 1. Time traces of the squared amplitudes of $\tilde{\phi}$ (A_p), \tilde{p}_e (A_n), and $\nabla_{\perp}^2 \tilde{\phi}$ (A_w). Due to the disparate k_{\perp} factors, A_p tracks mostly the flows and A_w mostly the turbulence. The basic slab case shows initial saturation and then weakening of the turbulence as the flow amplitude rises. The basic toroidal case shows persistent saturation, as the flow amplitude remains low.

We refer to the cases with $\omega_B = 0$ and 0.05 as the basic slab and toroidal cases, respectively. The time traces for these cases appear in Fig. 1. The squared amplitudes are shown for $\tilde{\phi}$ (A_p), \tilde{p}_e (A_n), and the vorticity $\nabla_{\perp}^2 \tilde{\phi}$ (A_w). When strong zonal flow layers appear, they dominate the A_p signal because of the lack of k_{\perp} factors. The A_w signal by contrast, with four additional k_{\perp} factors, mostly tracks the turbulence. For the basic slab case, the turbulence saturates in the time range $200 < t < 400$, after which it is ground down by the rise of the overall flow levels; A_p grows to large values, and A_w correspondingly decreases. For the basic toroidal case, the saturation occurs at roughly

the same time scale, but the Ap curve saturates unsteadily at a much lower level, smaller by about two orders of magnitude as in the slab case, reflecting the flows which are simply part of the turbulence. The turbulence saturates and maintains its level, close to the basic gyro Bohm transport. All time traces reflect this saturated state. We therefore find that the spin up and suppress scenario operates moderately well in slab geometry but not at all in toroidal geometry (for the same basic result in models including both temperatures see [19]).

The effort to explain this perhaps startling result forces systematic address of the various toroidal effects, all of which (in this model) operate through the curvature terms. There are two basic effects in the curvature operator \mathcal{K} : the interchange dynamics itself, and the geodesic curvature. Pure interchange dynamics operates on the $k_y \neq 0$ part, through $\mathcal{K}^y \partial / \partial y$. The geodesic curvature effect is in $\mathcal{K}^x \partial / \partial x$. To test directly for the geodesic curvature one must separate \mathcal{K}^x out for the $k_y = 0$ part and leave the \mathcal{K}^y pure interchange effect alone. The reason for suspecting the geodesic curvature is that the zonal flow effects lie in the $k_y = 0$ part, for which the pure interchange effect vanishes due to the vanishing $\partial / \partial y$.

The Geodesic Curvature Effect. The basic mode of oscillation involving the geodesic curvature is the classic MHD geodesic acoustic oscillation [20], which represents simple coupling between the pressure and vorticity through the geodesic curvature \mathcal{K}^x . The pressure part of this is a sideband with parallel wavenumber $k_{\parallel} q R = 1$ which presents itself as an interim free energy source to the turbulence. The potential part is the zonal flow; both are axisymmetric ($k_y = 0$). Due to the strong direct cascade tendency, the nonlinear ExB pressure advection, $\mathbf{v}_E \cdot \nabla \tilde{p}_e$, quickly delivers this free energy back to the turbulence. Overall, this transfer process acts as a depletion channel for zonal flow energy, keeping the zonal flow amplitude at levels comparable to the turbulence. The loss channel is from the zonal flow $\tilde{\phi}$ to the sideband \tilde{p}_e (the \mathcal{K}^x terms in Eqs. 1,3), and then through $\mathbf{v}_E \cdot \nabla \tilde{p}_e$ back to the eddies of the turbulence. The mutual energy transfer is conservative, so the tendency of the system to reach equipartition results in a finite population of the zonal flow mode, but not so large as to overwhelm the turbulence. We note that the fact that the geodesic curvature couples all k_{\parallel} modes of a given k_y requires us to keep or remove it for all $k_y = 0$ modes as a unit; otherwise, the resulting model would not conserve energy.

A modified toroidal case is constructed by taking \mathcal{K}^x out of the $k_y = 0$ part of the basic toroidal case, and a modified slab case is made by putting \mathcal{K}^x into the $k_y = 0$ part of the basic slab case, thereby isolating the geodesic curvature effects on the $k_y = 0$ part. The results concerning the turbulence amplitudes and transport are shown in Fig. 2. Two time traces are shown for each case: the transport (Qe) and the $\tilde{\phi}$ squared amplitude (Ap).

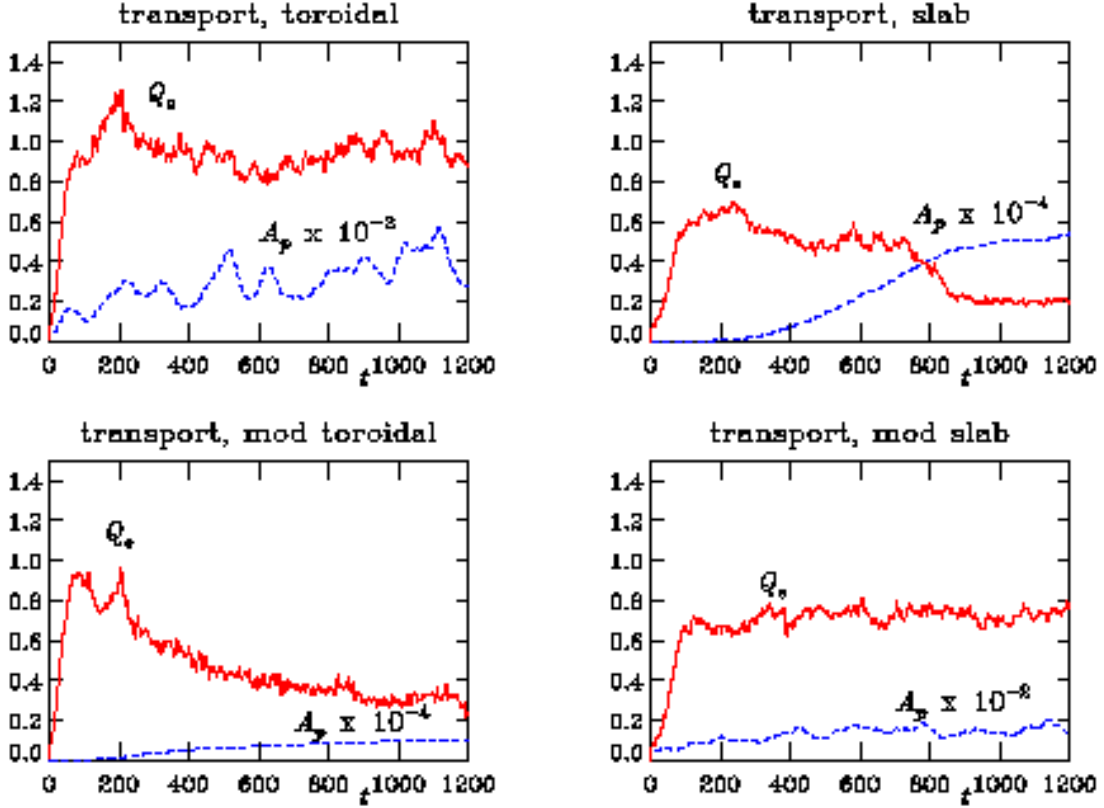


Figure 2. Time traces of the squared amplitudes of $\tilde{\phi}$ (A_p) and the transport (Q_e), for the four cases. The basic toroidal and modified slab cases reach persistent saturation; both contain the geodesic curvature effect. The basic slab and modified toroidal cases lack this effect and are both ground down by strong, self generated flow shear. This test confirms the geodesic curvature effect of coupling zonal flows to finite k_{\parallel} sidebands as the reason the spin up and suppress scenario does not work in toroidal geometry.

We find immediately that the two cases without geodesic curvature in the $k_y = 0$ part are similar, with the flow amplitude rising to high values, grinding down the transport. The two cases with the geodesic curvature in the $k_y = 0$ part are also similar, with the potential amplitude kept at levels low enough that the turbulence is not suppressed.

The morphology of $\tilde{\phi}$ and \tilde{p}_e is shown for the four cases in Fig. 3. The basic slab case shows dominance of the shear layer in the potential, with the vorticity disturbances stretched into thin sheets sharply tilted into the y -direction. The basic toroidal case also shows shear layers, but their vorticity represents a frequency not larger than that of

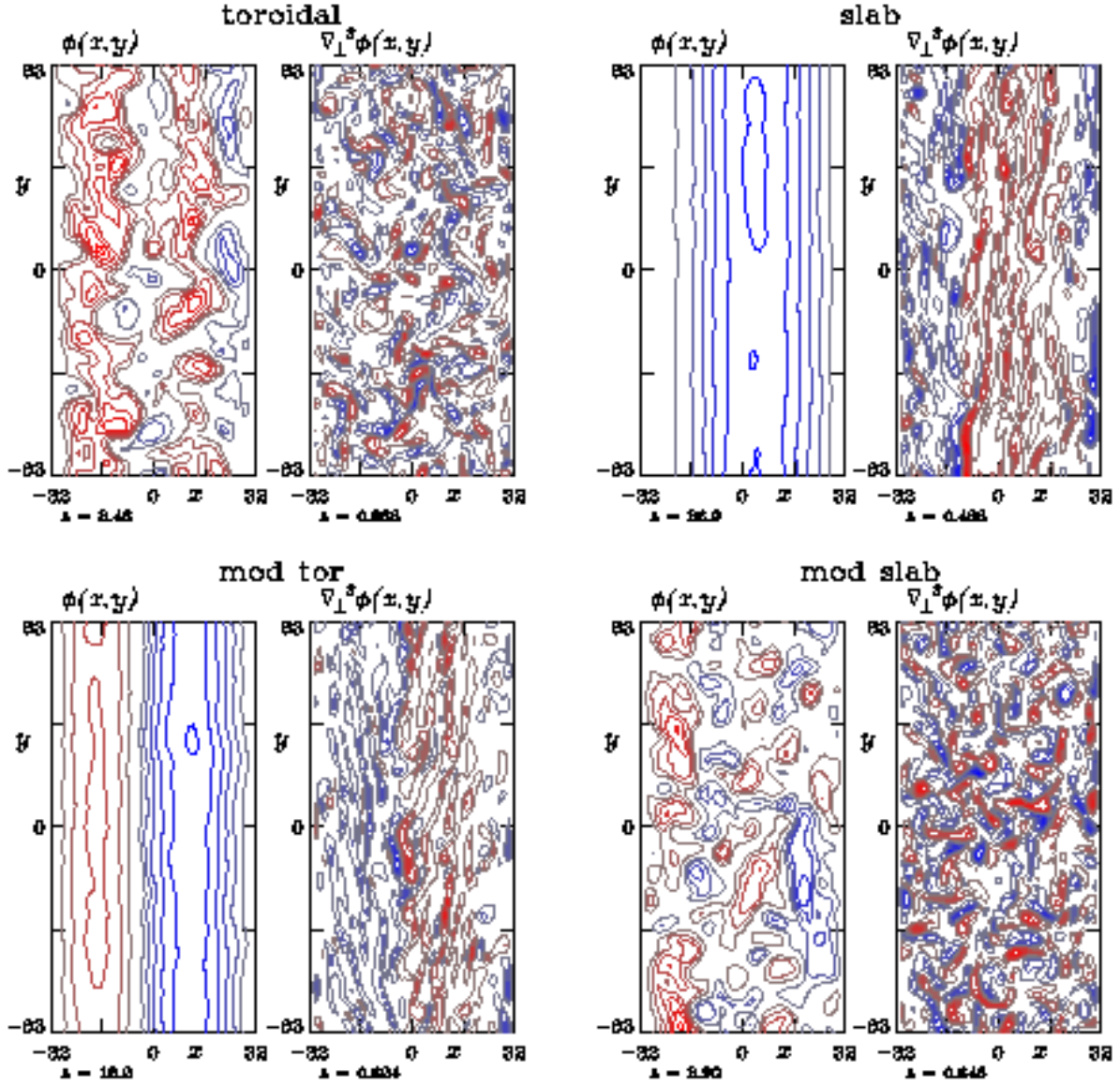


Figure 3. Morphology of the flows and disturbances (1/2 of the y -domain is shown). The basic slab case shows the strong shear layers in $\tilde{\phi}$, and sheets of vorticity ($\nabla_{\perp}^2 \tilde{\phi}$) stretched in the y -direction. The basic toroidal case shows visible shear layers in $\tilde{\phi}$, but they are of similar magnitude as the turbulence and do not strongly affect the form of $\nabla_{\perp}^2 \tilde{\phi}$. These are the time dependent zonal flow layers visible in the unsteady $\tilde{\phi}$ amplitude in Fig. 2. The modified toroidal case appears slablike, while the modified slab case looks like the basic toroidal case.

the basic turbulence, which is why a strong amount of suppression does not occur. The modified toroidal case shows the strong shear layer of the basic slab case, and the modified slab case shows the structure of the basic toroidal case. The shear levels of these weaker flows are comparable to the dynamical frequencies of the turbulence (about $0.1c_s/L_\perp$). The Ap curves for these two cases with weaker flows show those flows to be short-lived, comparable to the correlation time of the turbulence (about $6L_\perp/c_s$). These are the zonal flows which remain as part of the turbulence, leading in fact to moderate suppression but allowing it to remain at a robust amplitude.

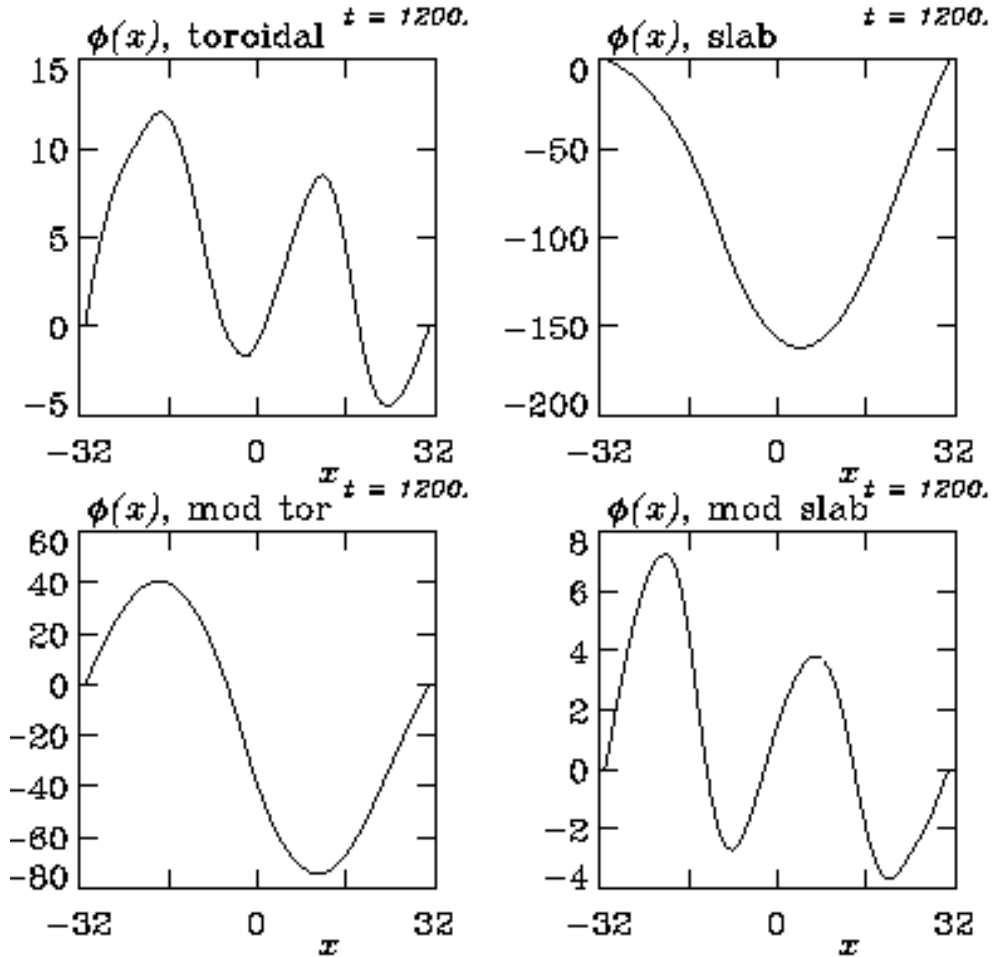


Figure 4. Snapshots of the zonal flow profiles for the four cases. The basic toroidal and modified slab cases show the weak, time dependent zonal flows which are part of the turbulence. The basic slab and modified toroidal cases show the strong, self generated shear layers which suppress the turbulence.

The instantaneous profiles (the zonal flow mode, $k_y = k_\parallel = 0$) of $\tilde{\phi}$ are shown for the

four cases in Fig. 4, in the same arrangement as for the time traces. The flow shear of these is strong or weak according to whether the geodesic curvature is absent or present in the $k_y = 0$ part, respectively. A rough guide of whether these sheared flow layers are able to suppress the turbulence is given by what can be called the “diamagnetic flow shear level” given by

$$\Omega_D = v_D/L_\perp \quad (9)$$

where $v_D = cT_e/eBL_\perp$ is the diamagnetic velocity. The level of shear in the $\tilde{\phi}$ profiles (actually given by the vorticity profile) is well below this for the two unsuppressed cases (basic toroidal and modified slab), and well above this for the other two cases. (ALT: show vor profiles, note diag shear is ρ_* in n.u., while turb omega is about 0.1)

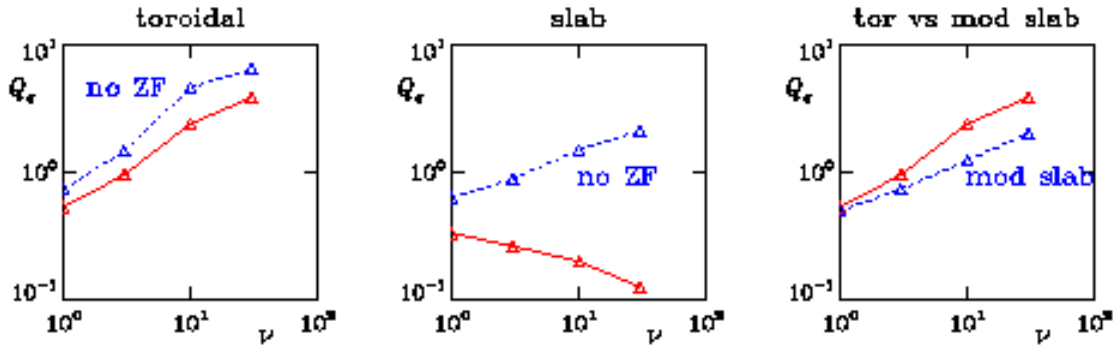


Figure 5. Transport trend versus collisionality. The drift wave regime extends to $\nu = 10$, at which $C\omega_B \approx 1$, and for these parameters the standard ν_* is 136. The basic toroidal and slab cases are compared to companion runs in which the zonal flow drive is removed. The time dependent zonal flows are the difference in the toroidal case; the self generated shear layers, in the slab case. The comparison between the basic toroidal and modified slab cases shows the role of pure interchange forcing; the difference at $\nu = 3$ ($C = 7.65$) is about 20 percent.

The transport results for various collisionality are summarised in Fig. 5 (note $C = 2.55\nu$). The basic toroidal and slab cases show similar trends if zonal flows are eliminated entirely by removing the flux surface average of $\mathbf{v}_E \cdot \nabla \nabla_\perp^2 \tilde{\phi}$. The fluctuating zonal flows provide a slightly reduced transport in the basic toroidal case, but the strong shear layers in the basic slab case strongly suppress the turbulence, even more so for larger C . The modified slab case is much like the basic toroidal case, showing the effects of geodesic

curvature to inhibit the strong shear layers, leaving the fluctuating zonal flows and the pure interchange effects intact. The small difference between those two cases is the pure interchange effect, incidentally showing that direct interchange drive in toroidal geometry is but a small perturbation on an existing drift wave mode structure.

The coupling of zonal flows to geodesic acoustic oscillations can be further demonstrated through the energy theorem satisfied by the zonal flows and the pressure sidebands. Let $\langle \dots \rangle$ denote the flux surface average and note that it commutes with $\partial/\partial x$ but annihilates $\partial/\partial y$. Let $\{ \dots \}$ further denote the average over x . The zonal flow potential is $\langle \phi \rangle$, the zonal flow is $\langle v^y \rangle = \langle \partial \phi / \partial x \rangle$, the zonal vorticity is $\langle \Omega \rangle = \langle \partial v^y / \partial x \rangle$, and the zonal flow energy is $\left\{ \langle v^y \rangle^2 \right\}$. Through the geodesic curvature the zonal flow is coupled to the Pfirsch-Schlüter Alfvén mode and then again to modifications in the background pressure (assuming unit diagonal metric, and neglecting sound waves, magnetic nonlinearities, and sidebands with $|k_{\parallel} q R| > 1$):

$$\frac{\partial}{\partial t} \left\{ \frac{1}{2} \langle v^y \rangle^2 \right\} = \{ \langle \Omega \rangle \langle v^x v^y \rangle \} - \omega_B \{ \langle p_e \sin s \rangle \langle v^y \rangle \} \quad (10)$$

$$\begin{aligned} \frac{\partial}{\partial t} \left\{ \langle p_e \sin s \rangle^2 \right\} &= 2 \left\{ \left\langle \frac{\partial p_e}{\partial x} \sin s \right\rangle \langle Q^x \sin s \rangle \right\} + \omega_B \{ \langle p_e \sin s \rangle \langle v^y \rangle \} \\ &\quad - \omega_B \left\{ \langle p_e \sin s \rangle \left\langle \frac{\partial p_e}{\partial x} \right\rangle \right\} - 2 \{ \langle p_e \sin s \rangle \langle J_{\parallel} \cos s \rangle \} \end{aligned} \quad (11)$$

$$\begin{aligned} \frac{\partial}{\partial t} \left\{ \hat{\beta}^{-1} \langle B^y \cos s \rangle^2 + \hat{\mu} \langle J_{\parallel} \cos s \rangle^2 \right\} \\ = 2 \{ \langle J_{\parallel} \cos s \rangle \langle (p_e - \phi) \sin s \rangle \} - 2C \left\{ \langle J_{\parallel} \cos s \rangle^2 \right\} \end{aligned} \quad (12)$$

$$\begin{aligned} \frac{\partial}{\partial t} \left\{ \langle v^y \sin s \rangle^2 \right\} &= 2 \{ \langle \Omega \sin s \rangle \langle v^x v^y \sin s \rangle \} \\ &\quad + \omega_B \left\{ \left\langle \frac{\partial p_e}{\partial x} \right\rangle \langle \phi \sin s \rangle \right\} + 2 \{ \langle \phi \sin s \rangle \langle J_{\parallel} \cos s \rangle \} \end{aligned} \quad (13)$$

$$\frac{\partial}{\partial t} \left\{ \frac{1}{2} \langle p_e \rangle^2 \right\} = \left\{ \left\langle \frac{\partial p_e}{\partial x} \right\rangle \langle Q^x \rangle \right\} - \omega_B \left\{ \left\langle \frac{\partial p_e}{\partial x} \right\rangle \langle (\phi - p_e) \sin s \rangle \right\} \quad (14)$$

where $Q^x = p_e v^x$ is the pointwise transport and $B^y = -\beta \partial A_{\parallel} / \partial x$ is the field disturbance. If time averages are taken, the left sides of these equations vanish and the right sides become balances between drive, transfer, and depletion mechanisms. The drive for the zonal flow is the zonally averaged Reynolds stress $\langle v^x v^y \rangle$, correlated with the zonal vorticity. The depletion mechanism is geodesic transfer to the Pfirsch-Schlüter sideband $\langle p_e \sin s \rangle$, and the depletion for that is the nonlinear transfer of free energy back to the turbulence (which requires nonadiabatic electrons, enabled by the finite $\hat{\beta}$). The flow sideband $\langle v^y \sin s \rangle$ is

controlled by relaxation of the Pfirsch-Schlüter current $\langle J_{\parallel} \cos s \rangle$. The proper geodesic acoustic oscillation is that between $\langle \phi \rangle$ and $\langle p_e \sin s \rangle$ as correctly noted in [20], the only subsystem not strongly affected by the Alfvén dynamics. We recognise $\{\langle \partial p_e / \partial x \rangle \langle Q^x \rangle\}$ as the negative of the main drive of the self sustained turbulence (cf. [21]), and hence as the corresponding depletion of the background $\langle p_e \rangle$. The profile is maintained by the damping of the $k_y = 0$ part of \tilde{p}_e to zero at the boundaries in x , which affects both $\langle p_e \rangle$ and $\langle p_e \sin s \rangle$. For the nominal case the zonal Reynolds stress and geodesic transfer were measured at 0.858 ± 0.359 and 1.02 ± 0.305 , and depletion of the sideband went through the nonlinearity, the profile maintenance, and the Pfirsch-Schlüter transfer to the background at 0.470 ± 0.431 and 0.301 ± 0.100 and 0.103 ± 0.0741 , respectively, with all other sideband effects much smaller (all numbers $\times 10^{-2}$). The nonlinear depletion of $\langle p_e \sin s \rangle$ functions because of the pointwise correlation of Q^x with $-\partial p_e / \partial x$. Indeed, while either of these two $\sin s$ terms is small in time average, the average of their product is not, because of this correlation. This energetic depletion therefore overwhelms any slight presence of a nonzero $\langle Q^x \sin s \rangle$ (Stringer-Taylor effect). Indeed, the PDF of $\langle Q^x \sin s \rangle$ was found to be close to Gaussian. The pressure nonlinearity is therefore a depletion of the sideband and therefore ultimately of the zonal flow. The energy flow is $\tilde{p}_e \rightarrow \langle \phi \rangle \rightarrow \langle p_e \sin s \rangle \rightarrow \tilde{p}_e$, through the Reynolds stress, geodesic curvature, and nonlinear flux correlation, respectively. The Stringer-Taylor effect is therefore a *sink* for the zonal flow system, not a source as incorrectly reported in Ref. [22], whose runs were apparently not taken to complete statistical saturation and in any case suffer from all the shortcomings of the drift resistive ballooning paradigm (cf. Ref. [18]).

Main Points. The principal result of this study is that while the turbulent Reynolds stress always tends towards a transfer of energy from small eddies to the larger scale zonal flows (similar k_x but disparate k_y), in toroidal geometry the geodesic curvature couples the zonal flows to finite- k_{\parallel} pressure sidebands, which act as a loss channel by means of nonlinear advective transfer back to the turbulence. This prevents large scale, large amplitude zonal flows from forming and therefore rules out the spin up and suppress scenario for transport barrier formation, at least due to local (homogeneous) action of the ExB Reynolds stress. The ExB shear layers observed in tokamak edge transport barriers [12] must therefore come from some other mechanism, most likely having to do with the neoclassical equilibrium. Two recent proposals are a generalised ion orbit loss mechanism [23,24], and the generation of a large parallel flow and its equilibrium electric field profile by coupling to the open field line regions [25]. For the core regions the electron response is more adiabatic and electrostatic, so that current results on core zonal flows [11] are not affected.

References

- [1] A. Hasegawa and K. Mima, *Phys. Rev. Lett.* **39** (1977) 205; *Phys. Fluids* **21** (1978) 87.
- [2] M. Wakatani and A. Hasegawa, *Phys. Fluids* **27** (1984) 611.
- [3] B. Scott, *Plasma Phys. Contr. Fusion* **39** (1997) 1635.
- [4] B. Scott, *New J. Phys.* **4** (2002) 52.
- [5] Reviewed by P. W. Terry, *Phys. Plasmas* **7** (2000) 1653.
- [6] H. Biglari, P. Diamond, and P. W. Terry, *Phys. Fluids B* **3** (1991) 1.
- [7] P. Diamond and Y. Kim, *Phys. Fluids B* **3** (1991) 1626.
- [8] R. Kraichnan, *Phys. Fluids* **10** (1967) 1417.
- [9] B. Scott, *Plasma Phys. Contr. Fusion* **34** (1992) 1977.
- [10] T. S. Hahm, M. A. Beer, Z. Lin, G. W. Hammett, W. W. Lee, and W. M. Tang, *Phys. Plasmas* **6** (1999) 922.
- [11] Z. Lin, T. S. Hahm, W. W. Lee, W. M. Tang, R. B. White, *Science* **281** (1998) 1835; also R. Sydora (get ref from Dimits).
- [12] H-Mode discovery: F. Wagner *et al*, *Phys. Rev. Lett.* **49** (1982) 1408; H-Mode morphology: P. Gohil, K. H. Burrell, E. J. Doyle, R. J. Groebner, J. Kim, and R. P. Seraydarian, *Nucl. Fusion* **34** (1994) 1057.
- [13] P. H. Diamond, Y.-M. Liang, B. A. Carreras, and P. W. Terry, *Phys. Rev. Lett.* **72** (1994) 2565.
- [14] B Scott, "Physics of Zonal Flows in Drift Wave Turbulence," in *Theory of Fusion Plasmas* (Editrice Compositori, Bologna, 2000, J. Connor, O. Sauter, and E. Sindoni, eds), p. 413; cf. also B. Scott, "Recent Results Concerning Local and Global Computation of Self-Consistent Transport Scenarios," in *Plasma Physics and Controlled Nuclear Fusion Research 1994*, Proceedings of the 15th International Conference, Seville (IAEA, Vienna, 1996), Vol. 3, p. 447.

- [15] B. Scott, *Phys. Plasmas* 8 (2001) 447.
- [16] B. Scott, *Phys. Plasmas* 5 (1998) 2334.
- [17] S. I. Braginskii, *Rev. Plasma Phys.* 1 (1965) 205.
- [18] B. Scott, preprint [arXiv:physics.plasm-ph/0207126](https://arxiv.org/abs/physics.plasm-ph/0207126), submitted to *Phys. Plasmas* .
- [19] B. Scott, *Phys. Plasmas* 7 (2000) 1845.
- [20] N. Winsor, J. Johnson, and J. Dawson, *Phys. Fluids* 11 (1968) 2448.
- [21] B. Scott, *Phys. Rev. Lett.* 65 (1990) 3289; *Phys. Fluids B* 4 (1992) 2468.
- [22] K. Hallatschek and D. Biskamp, *Phys. Rev. Lett.* 86 (2001) 1223.
- [23] K. C. Shaing and E. C. Crume, Jr., *Phys. Rev. Lett.* 63 (1989) 2369.
- [24] J. A. Heikkinen, T. P. Kiviniemi, and A. G. Peeters, *Phys. Rev. Lett.* 84 (2000) 487.
- [25] D. Morozov, V. Rozhansky, J. Herrera, and T. Soboleva, *Phys. Plasmas* 7 (2000) 1184.